Journal of Controlled Release 334 (2021) 201–212

Contents lists available at ScienceDirect

Journal of Controlled Release

journal homepage: www.elsevier.com/locate/jconrel

Fucosylated lipid nanocarriers loaded with antibiotics efficiently inhibit mycobacterial propagation in human myeloid cells

Verónica Durán [a,1], Elena Grabski [a,1,2], Constantin Hozsa [b], Jennifer Becker [a], Hanzey Yasar [c], João T. Monteiro [d,3], Bibiana Costa [a], Nicole Koller [e], Yvonne Lueder [f], Bettina Wiegmann [g,h,i], Gudrun Brandes [j], Volkhard Kaever [k], Claus-Michael Lehr [c], Bernd Lepenies [d], Robert Tampé [e], Reinhold Förster [f,m], Berislav Bošnjak [f,*], Marcus Furch [b,*], Theresa Graalmann [a,l,4,**], Ulrich Kalinke [a,m,4,**]

[a] Institute for Experimental Infection Research, TWINCORE, Centre for Experimental and Clinical Infection Research, a joint venture between the Hannover Medical School and the Helmholtz Centre for Infection Research, Hannover, Germany
[b] Rodos Biotarget GmbH, Hannover, Germany
[c] Helmholtz-Institute for Pharmaceutical Research Saarland (HIPS) – Helmholtz Center for Infection Research (HZI), Department of Drug Delivery (DDEL), Saarbrücken, Germany
[d] Institute for Immunology & Research Center for Emerging Infections and Zoonoses (RIZ), University of Veterinary Medicine Hannover, Hannover, Germany
[e] Institute of Biochemistry, Biocenter, Goethe University Frankfurt, Frankfurt, Germany.
[f] Institute of Immunology, Hannover Medical School, Hannover, Germany.
[g] Department of Cardiothoracic, Transplantation and Vascular Surgery, Hannover Medical School, Hannover, Germany.
[h] Lower Saxony Center for Biomedical Engineering, Implant Research and Development, Hannover, Medical School, Germany
[i] German Centre of Lung Research, 30625, Hannover, Germany
[j] Institute of Neuroanatomy and Cell Biology, Hannover Medical School, Hannover, Germany.
[k] Institute of Pharmacology, Hannover Medical School, Hannover, Germany.
[l] Clinic of Immunology and Rheumatology, Hannover Medical School, Hannover, Germany.
[m] Cluster of Excellence – Resolving Infection Susceptibility (RESIST), Hannover Medical School, Hannover, Germany.

ARTICLE INFO

Keywords:
Tuberculosis
Alveolar macrophages
Targeted drug delivery
Liposomes
Nanomedicine

ABSTRACT

Antibiotic treatment of tuberculosis (TB) is complex, lengthy, and can be associated with various adverse effects. As a result, patient compliance often is poor, thus further enhancing the risk of selecting multi-drug resistant bacteria. Macrophage mannose receptor (MMR)-positive alveolar macrophages (AM) constitute a niche in which *Mycobacterium tuberculosis* replicates and survives. Therefore, we encapsulated levofloxacin in lipid nanocarriers functionalized with fucosyl residues that interact with the MMR. Indeed, such nanocarriers preferentially targeted MMR-positive myeloid cells, and in particular, AM. Intracellularly, fucosylated lipid nanocarriers favorably delivered their payload into endosomal compartments, where mycobacteria reside. In an in vitro setting using infected human primary macrophages as well as dendritic cells, the encapsulated antibiotic cleared the pathogen more efficiently than free levofloxacin. In conclusion, our results point towards carbohydrate-functionalized nanocarriers as a promising tool for improving TB treatment by targeted delivery of antibiotics.

* Corresponding authors.
** Corresponding authors at: Institute for Experimental Infection Research, TWINCORE, Centre for Experimental and Clinical Infection Research, a joint venture between the Hannover Medical School and the Helmholtz Centre for Infection Research, Hannover 30625, Germany.
E-mail addresses: bosnjak.berislav@mh-hannover.de (B. Bošnjak), m.furch@biotargeting.eu (M. Furch), theresa.graalmann@twincore.de (T. Graalmann), ulrich.kalinke@twincore.de, kalinke.office@twincore.de (U. Kalinke).
[1] Equally contributing first authors.
[2] Present address: Division of Virology, Section Viral Vaccines, Paul Ehrlich Institute, Federal Institute for Vaccines and Biomedicines, Langen, Germany.
[3] Present address: Department of Pediatric Pneumology, Allergology and Neonatology, Hannover, Germany.
[4] Equally contributing last authors.

https://doi.org/10.1016/j.jconrel.2021.04.012
Received 21 August 2020; Received in revised form 10 April 2021; Accepted 12 April 2021
Available online 16 April 2021

1. Introduction

Tuberculosis (TB) is one of the top ten causes of deaths worldwide. Although already discovered in the 1880s, *Mycobacterium tuberculosis* (Mtb), the causative agent of TB, still kills more people annually than any other infectious agent [1]. For treatment of drug-sensitive TB, patients are typically prescribed with a standard 6-months course of four antibiotics: isoniazid, rifampicin, ethambutol, and pyrazinamide [2]. This elaborate scheme is often associated with low patient compliance, which leads to treatment failure and an enhanced risk for the emergence of multi-drug resistant (MDR) as well as extensively-drug resistant (XDR) Mtb strains [2]. In 2017, an estimate of 18% MDR-TB and 8.5% XDR-TB cases were reported, from the total of treated TB patients who showed re-emergence of TB [3]. For these reasons, the development of novel TB drug regimens that aim for shorter and simpler treatments, while being more efficacious and generating fewer side effects is a global medical priority. Ideally, these new treatments should also be applicable against multi-resistant Mtb strains.

As TB primarily affects the lung, there has been an increasing interest in developing localized drug delivery formulations for improving the current regimens [4–6]. Targeting alveolar macrophages (AM) is particularly attractive, as these cells serve as the main site of early Mtb infection and dissemination [7], as well as a niche where the bacterium is able to hide, avoid lysosomal acidification, and evade immune responses [8–10]. Therefore, AM serve not only as a first line of defense but also constitute an attractive target for cell-selective drug delivery.

AM express various C-type lectin receptors (CLR), which allow them to selectively interact with glycan-expressing pathogens such as Mtb [11,12]. The advantages of targeting myeloid cells via CLR have been broadly studied in the context of cancer and infection therapies [13,14], vaccine development [15], and immunotherapies [16]. Already in 1997, Shao and Ma highlighted the potential of targeting AM by exploiting a carbohydrate ligand that interacts with high affinity with the macrophage mannose receptor (MMR) [17]. The MMR is a mannose/fucose-binding CLR that is highly expressed on AM and mediates the initial recognition and phagocytosis of Mtb [18–20]. Although previous investigations followed the approach of targeting AM via the MMR [21–23], to date there is no comprehensive study addressing the targeting mechanism and the drug delivery potential of CLR-targeting nanocarriers. Hence, in this study we evaluated the potency of fucosylated lipid nanocarriers to target MMR-positive myeloid cells, such as AM, and to selectively deliver levofloxacin to these cells as an innovative approach to treat Mtb infection. Here we show that these nanocarriers, also called CLR-TargoSpheres [24], were mainly taken up by MMR-mediated endocytosis in macrophages and other myeloid cell subsets, and that they preferentially reached endosomal compartments. When applied to human primary myeloid cells, levofloxacin encapsulated in fucosylated lipid nanocarriers inhibited mycobacterial growth more effectively than free levofloxacin, endorsing the potential of carbohydrate-functionalized nanocarriers as an innovative drug delivery approach for TB treatment.

2. Results

2.1. Human alveolar macrophages express high levels of C-type lectin receptors

C-type lectin receptors (CLR) play a key role in the initial recognition of the glycan-rich cell wall of Mtb [25]. Therefore, we analyzed the CLR expression profiles of human lung immune cell subsets. To this end, explanted lung tissue obtained from lung transplant recipients was enzymatically digested, single cell suspensions were prepared, and neutrophils ($CD45^+MHC\text{-}II^{low}CD15^+$), monocytes ($CD45^+MHC\text{-}II^+CD15^-CD11b^+Siglec\text{-}1^-MMR^-$), interstitial macrophages (IM, $CD45^+MHC\text{-}II^+CD15^-CD11b^+Siglec\text{-}1^{low}MMR^{low}$) and alveolar macrophages (AM, $CD45^+MHC\text{-}II^+CD15^-CD11b^+Siglec\text{-}1^{high}MMR^{high}$) were analyzed (Fig. 1A). The expression profiles for MMR (CD206), DEC-205 (CD205), and DC-SIGN (CD209) were characterized by flow cytometry and calculated as fold increase in mean fluorescence intensity (MFI) above the isotype background. We found DEC-205 to be moderately expressed only on monocytes with a 1.5-fold increased MFI, whereas AM showed moderate DC-SIGN (1.6-fold) and abundant MMR expression (10-fold) (Fig. 1B, C). Thus, high MMR expression is suited to distinguish AM from other lung-resident myeloid cell subsets.

2.2. Characterization and physicochemical properties of fucosylated lipid nanocarriers

To target AM for TB treatment, we used lipid nanocarriers functionalized with fucosyl residues and loaded with levofloxacin (Fig. 2A), and we extensively characterized their physicochemical properties (Fig. 2B). Transmission electron microscopy of negative-stained nanocarriers verified their evenly distributed, spherical morphology and precluded any formation of aggregates. By dynamic light scattering (DLS), a mean nanoparticle diameter of 109 ± 8 nm was determined, whereas a polydispersity index (PDI) of 0.12 indicated a homogeneous size distribution. Furthermore, a ζ-potential of −6.6 mV (in PBS at pH 7.4) revealed a slightly negative charge (Fig. 2B). Next, we characterized the properties of the fucosyl groups displayed on the surface of the lipid nanocarriers. To this end, such lipid nanocarriers were incubated with FITC-coupled *Aleuria aurantia* lectin (AAL), which binds specifically to fucosyl motifs. After washing, FITC fluorescence was determined by flow cytometry and non-targeted nanocarriers were employed as controls. In contrast to non-functionalized control nanocarriers, almost 100% of fucosylated lipid nanocarriers were FITC-positive after incubation with 20 μg/μl AAL, thus confirming their successful functionalization (Fig. 2C-E). Moreover, the binding profile to different CLRs was analyzed by flow cytometry using CLR-hFc fusion proteins [26–28]. DC-SIGN, a fucose-binding CLR, showed the highest binding to fucosylated lipid nanocarriers with a 11-fold increased MFI above background, followed by MGL with an 8-fold increase, whereas CLEC12B and DCAR had the lowest binding with 2.7- and 1.5-fold increased MFI, respectively (Fig. 2F, G). These results confirmed the preferred interaction of lipid nanocarriers with fucose-binding CLR.

2.3. C-type lectin receptor expression profiles of primary human immune cell subsets

Due to the limited availability of human lung tissue, we used primary human immune cells derived from blood, including human peripheral blood mononuclear cells (PBMC) as well as monocyte-derived macrophages (moMΦ) and dendritic cells (moDC) to study CLR expression. Within PBMC, we identified T and B cells as $CD3^+CD19^-$ and $CD19^+CD3^-$, respectively, whereas within the $CD3^-CD19^-$ population monocytes were defined as $MHC\text{-}II^+CD14^+$ and dendritic cells (DC) as $MHC\text{-}II^+CD14^-$ (Fig. 3A). To generate monocyte-derived antigen-presenting cells, $CD14^+$ cells isolated from PBMC were cultivated in medium supplemented with M-CSF or the combination of GM-CSF and IL-4 for differentiation of moMΦ and moDC, respectively. Of all investigated cells, monocytes showed the highest expression of DEC-205 with a 16-fold increased MFI above isotype background, followed by blood DC (14-fold) and moDC (7-fold). In contrast, T cells did not express DEC-205, while B cells and moMΦ showed moderate DEC-205 expression (4-fold) (Fig. 3B, C). Similarly, amongst PBMC, MMR expression was not detectable on T cells, whereas B cells showed moderate MMR expression (4-fold) and monocytes (13-fold) and blood DC (16-fold) showed high MMR expression (Fig. 3B, C). Interestingly, on moMΦ and moDC the MMR expression was even higher, with 44-fold and 54-fold increased MFI above background, respectively (Fig. 3B, C). Finally, DC-SIGN expression was absent on all immune cell subsets amongst PBMC, whereas moMΦ showed high (14-fold) and moDC even higher (60-fold) DC-SIGN expression (Fig. 3B, C). Thus, DEC-205 expression is detected

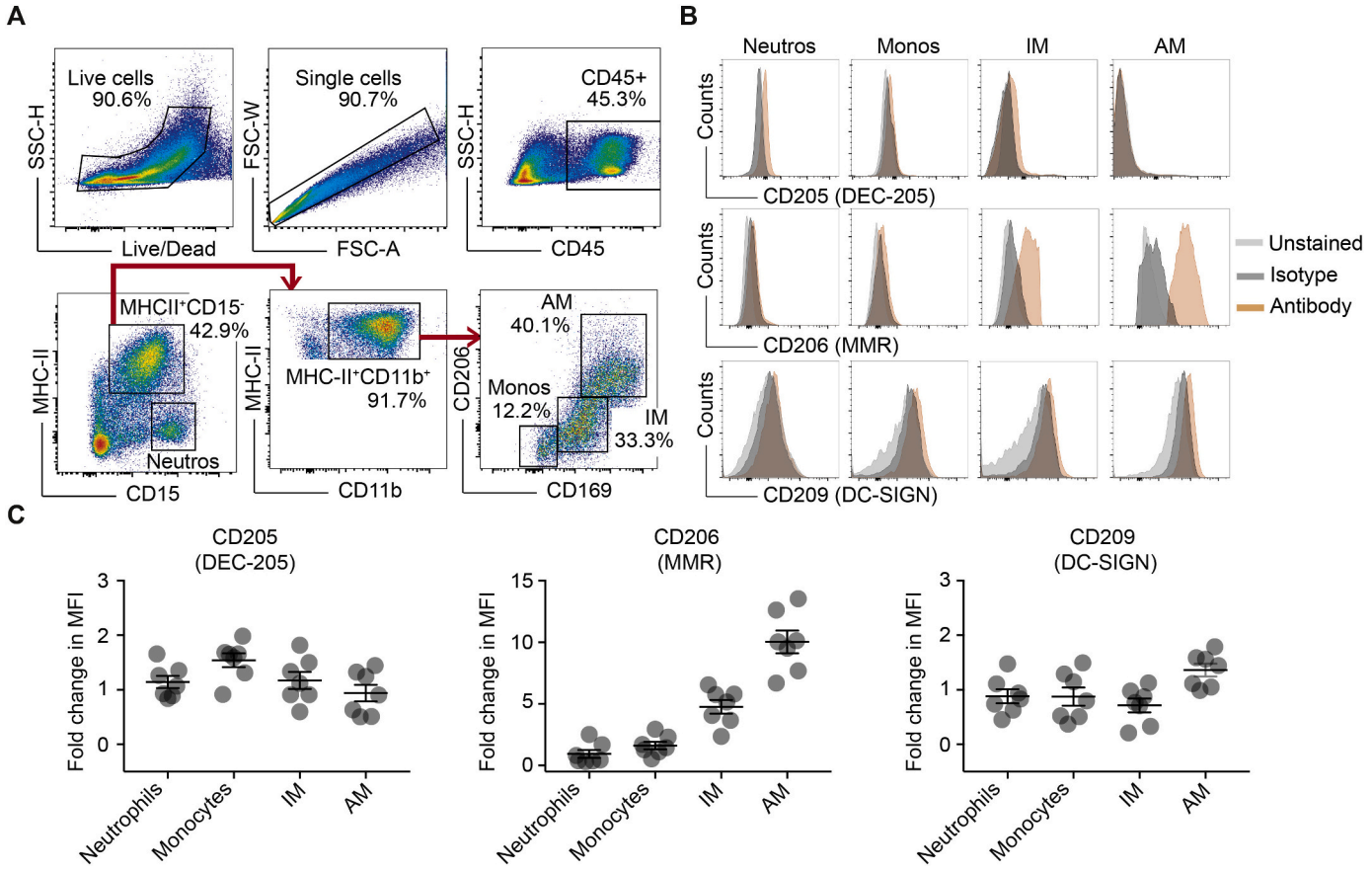

Fig. 1. Alveolar macrophages isolated from human lung samples show abundant expression of the macrophage mannose receptor (MMR). (A) $CD45^+MHC\text{-}II^{low}CD15^+$ neutrophils, $CD45^+MHC\text{-}II^+CD15^-CD11b^+Siglec\text{-}1^-MMR^-$ monocytes, $CD45^+MHC\text{-}II^+CD15^-CD11b^+Siglec\text{-}1^{low}MMR^{low}$ interstitial macrophages (IM), and $CD45^+MHC\text{-}II^+CD15^-CD11b^+Siglec\text{-}1^{high}MMR^{high}$ alveolar macrophages (AM) were gated within single-cell preparations of human lung tissue, as indicated for one representative donor. (B) The expression profiles for CD205 (DEC-205), CD206 (MMR) and CD209 (DC-SIGN) were characterized on neutrophils, monocytes, interstitial macrophages (IM) and alveolar macrophages (AM). Histograms show surface expression for one representative donor. (C) Quantification of the fold-increase in mean fluorescence intensity (MFI) above background (isotype sample) *(n = 7)*.

on various immune cell subsets, including B cells and myeloid cells, whereas MMR is exclusively expressed on myeloid cells, and DC-SIGN is primarily expressed on monocyte-derived cells.

2.4. Amongst PBMC and lung derived immune cells, myeloid cells show enhanced uptake of fucosylated lipid nanocarriers

To study the uptake of fucosylated lipid nanocarriers by human primary PBMC, cells were treated for 2 h at 37 °C with Texas Red-labeled nanocarriers. Pre-incubation with soluble L-fucose was used as a control to block fucose-binding CLR. Additionally, incubation at 4 °C was performed because at this temperature no active phagocytosis occurs, which allows us to assess the binding of nanocarriers to the cell surface. After identifying cellular subsets within PBMC by immunolabeling (Fig. 3A), the percentage of Texas Red-positive cells was determined by flow cytometry as a measure of nanocarrier uptake. Neither T nor B cells showed significant uptake of fucosylated nanocarriers under any of the tested conditions (Fig. 4A). Within myeloid cells, approx. 40% of the blood DC showed uptake of fucosylated nanocarriers, which decreased to approx. 20% in the presence of 1 mM L-fucose. This effect was even enhanced in the case of monocytes, where the uptake decreased from 70% to 40% after CLR blocking with soluble L-fucose. Thus, within PBMC myeloid cells, including monocytes and DC, but not lymphocytes, showed enhanced uptake of fucosylated lipid nanocarriers, which was significantly reduced by blocking fucose-binding CLR (Fig. 4A).

We further determined the uptake of fucosylated lipid nanocarriers in cells isolated from secondary lymphoid organs including tonsils and lymph nodes (Supplementary Fig. 1A), as well as from human lung tissue (Fig. 4B). Amongst secondary lymphoid organs, DC showed the highest nanocarrier uptake with approx. 50% Texas Red-positive cells within tonsils and 37% positive cells within lymph nodes (Supplementary Fig. 1B). In lung tissue, approx. 65% of neutrophils showed nanocarrier uptake, and within the pulmonary macrophage subsets, AM showed the highest uptake with approx. 54% Texas Red-positive cells, followed by IM with 47% and monocytes with 25% positive cells. Interestingly, fucose blocking in this case did not affect the uptake of the fucosylated nanocarriers by any of these cell subsets. Thus, within the lung, fucosylated lipid nanocarriers preferentially targeted neutrophils and AM.

2.5. Fucosylated lipid nanocarriers are preferentially trafficked to endosomal compartments via fucose-binding C-type lectin receptors

To study the subcellular localization of fucosylated lipid nanocarriers, moMΦ were incubated for 2 h at 37 °C with Texas Red-labeled nanocarriers, with or without pre-incubation with soluble L-fucose. After fixation, markers for intracellular organelles including Rab5 for early endosomes, Rab7 for late endosomes, Lamp1 for lysosomes, Rab11 for recycling endosomes, GM130 for the Golgi apparatus, and calnexin for the endoplasmic reticulum were immunolabeled (Fig. 5, A and B). Confocal microscopy was performed and images were further mathematically analyzed to determine the colocalization of Texas Red fluorescence derived from internalized nanocarriers and the labeled respective subcellular compartments, as reflected by the Pearson's correlation coefficient (PCC) [29].

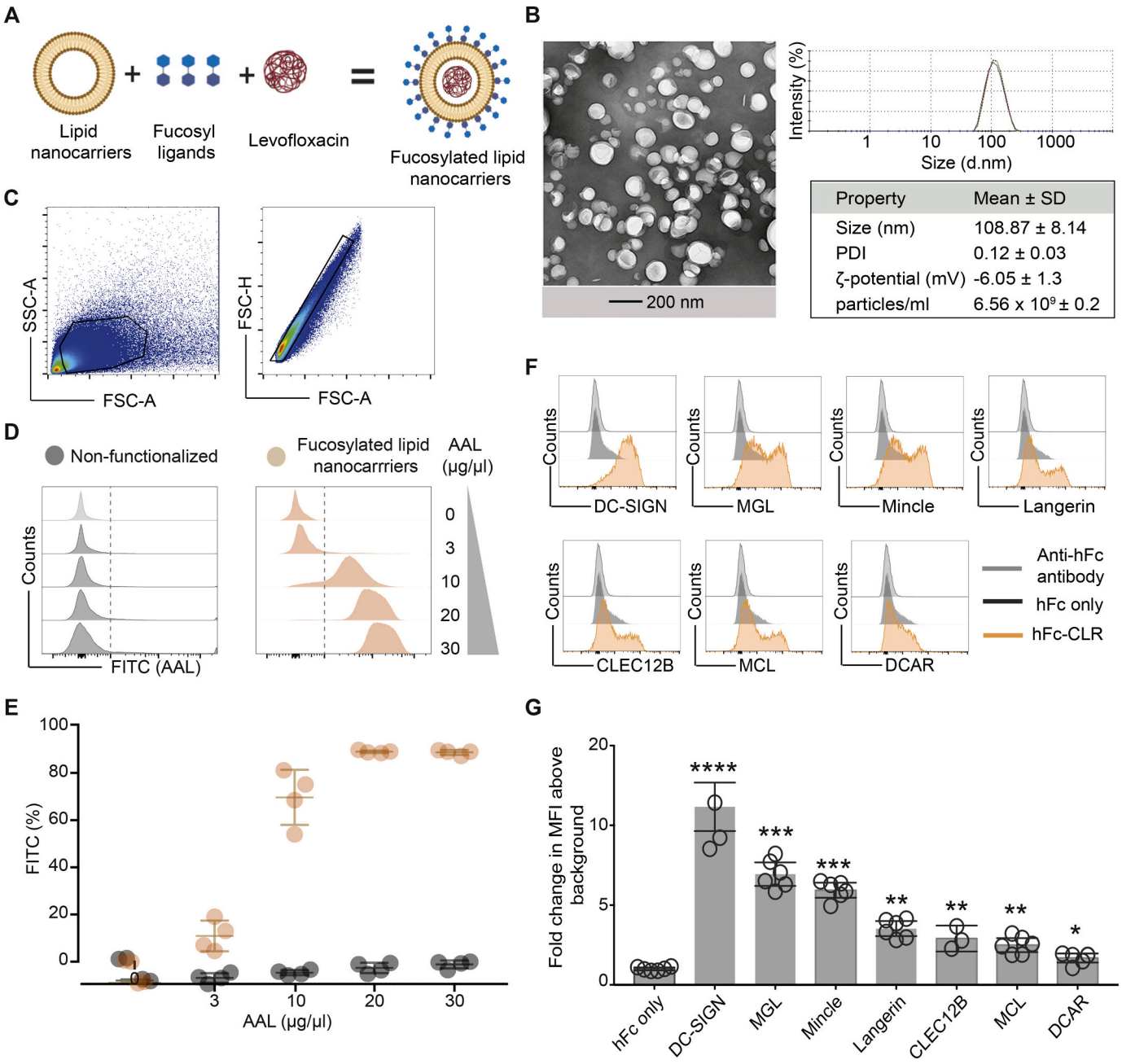

Fig. 2. Characterization and physicochemical properties of fucosylated lipid nanocarriers. (A) Schematic depiction of fucosylated lipid nanocarriers. Created with Biorender.com (B) Transmission electron micrographs of fucosylated lipid nanocarriers and physicochemical properties as measured by dynamic light scattering (DLS). Data are presented as means ± SD ($n = 4$). Fucosylated lipid nanocarriers as well as non-targeted nanocarriers were incubated for 20 min at 4 °C with the FITC-coupled, fucose-binding *Aleuria aurantia* lectin (AAL) and the FITC signal was determined by flow cytometry. (C) Gating strategy and (D) histograms from a representative replicate for each nanocarrier preparation are shown. (E) Quantification of the mean fluorescence intensity (MFI) from 4 nanocarrier batches. Error bars indicate means ± SD. Fucosylated lipid nanocarriers were incubated with different C-type lectin receptor (CLR)–hFc fusion proteins in solution for 1 h at 4 °C. Binding was measured by flow cytometry using an anti-hFc antibody. (F) Histograms depict representative MFI for each CLR-hFc construct. (G) Values plotted correspond to fold change in MFI above background (hFc only control). DC-SIGN: dendritic cell-specific intercellular adhesion molecule-3-grabbing non-integrin; MGL: macrophage galactose binding lectin; Mincle: macrophage inducible $Ca2^{+}$-dependent lectin receptor; MCL: macrophage C-type lectin, also called Clec4d; DCAR: dendritic cell immunoactivating receptor. Error bars indicate means ± SEM, two-tailed unpaired *t*-test, $^{****}P \leq 0.0001$, $^{***}P \leq 0.0003$, $^{**}P \leq 0.0019$, $^{*}P \leq 0.0289$, $n = 6$, $N = 2$.

Fucosylated lipid nanocarriers highly colocalized with endosomal compartments and this effect was significantly reduced upon CLR blocking with L-fucose. In the case of early endosomes, the PCC decreased from 0.38 to 0.11. For late endosomes, the PCC decreased from 0.34 to 0.16, and for lysosomes it decreased from 0.25 to 0.14. In contrast, colocalization with the endoplasmic reticulum and recycling endosomes was moderate (PCC 0.2 and 0.17, respectively). Finally, no significant colocalization was detected with the Golgi apparatus (Fig. 5C). Thus, these results support the hypothesis that after cellular uptake via carbohydrate-binding CLR, fucosylated lipid nanocarriers are trafficked to endosomal compartments.

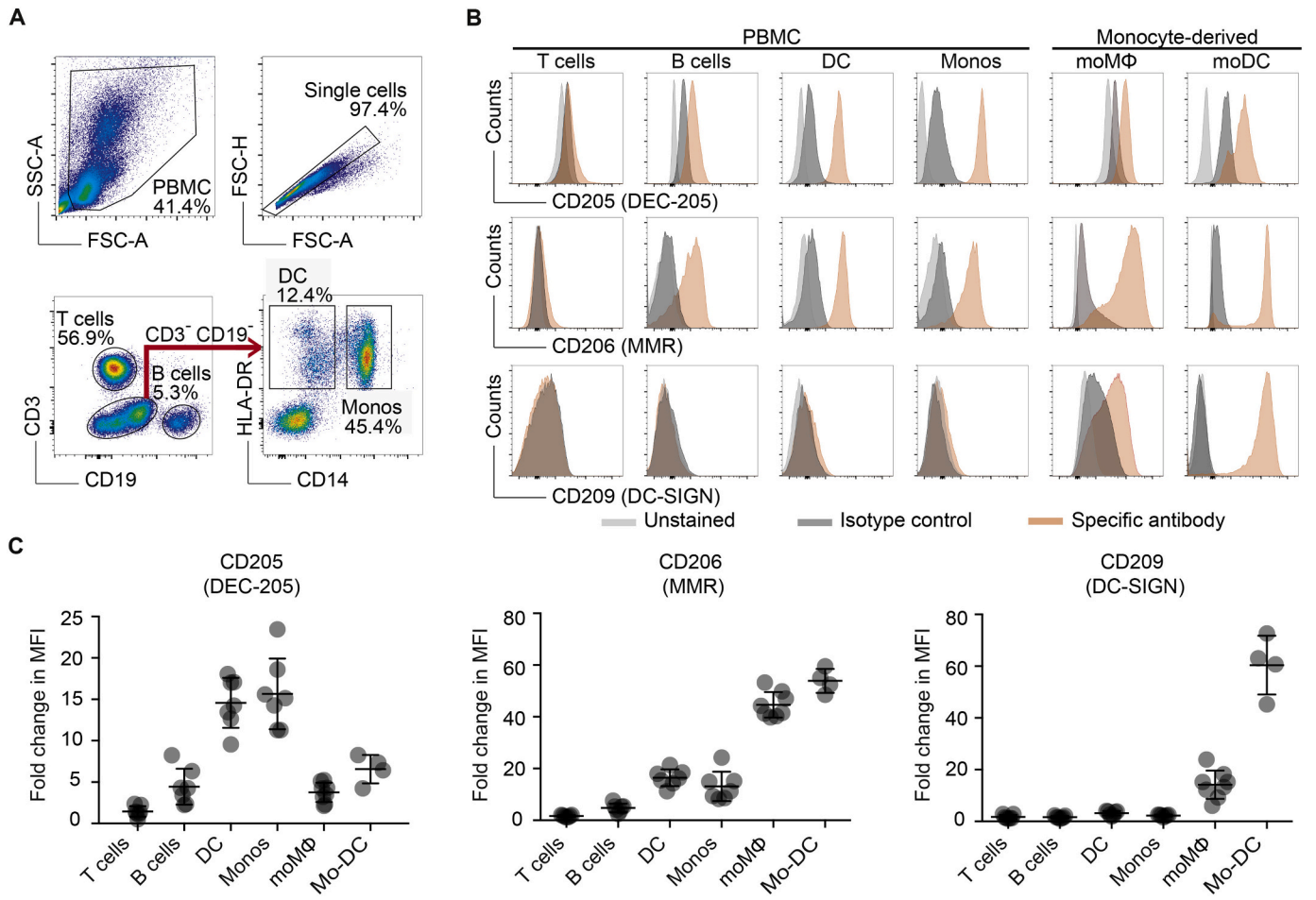

Fig. 3. C-type lectin receptor expression profiles of immune cell subsets within human PBMC. (A) $CD3^{+}CD19^{-}$ T cells, $CD3^{-}CD19^{+}$ B cells, $CD3^{-}CD19^{-}MHCII^{+}CD14^{+}$ monocytes and $CD3^{-}CD19^{-}MHCII^{+}CD14^{-}$ dendritic cells (DC) were gated within human PBMC as indicated for one representative donor. (B) PBMC as well as monocyte-derived macrophages (moMΦ) and dendritic cells (moDC) were immunolabeled for CD205 (DEC-205), CD206 (MMR) and CD209 (DC-SIGN). Histograms depict surface expression for one representative donor. (C) Values shown correspond to fold-increase in mean fluorescence intensity (MFI) above background (isotype sample) ($n = 4–7$, $N > 3$).

2.6. MMR-dependent uptake delivers fucosylated lipid nanocarriers to endosomal compartments

To further elucidate the role of fucose-binding CLR in the uptake of fucosylated lipid nanocarriers, we performed a CRISPR/Cas9 gene knock-out of the MMR in human moMΦ and evaluated the intracellular localization of such nanocarriers upon internalization. To this end, we used two different guide RNAs (gRNA) that target the *mrc1* gene encoding the human MMR (*mrc1* #1 and #2) as well as an irrelevant control gRNA that does not target any human gene, and prepared the corresponding Cas9 ribonucleoparticles (RNP). Such RNP containing either *mrc1* #1 and #2 gRNA individually or in combination were nucleofected into freshly isolated monocytes, and the cells were differentiated for 5 days in M-CSF supplemented medium to generate moMΦ (Fig. 6A). Flow-cytometric analysis revealed that monocytes nucleofected with either *mrc1* #1 or *mrc1* #2 RNPs showed deletion of the MMR expression in approx. 50% of the moMΦ (Fig. 6B). When both *mrc1* #1 and *mrc1* #2 RNPs were nucleofected simultaneously, >90% of the moMΦ showed MMR deletion, which was confirmed at the protein level by western blot analysis (Fig. 6C). Next, confocal microscopy analysis was performed to determine the subcellular localization of fucosylated lipid nanocarriers in MMR-negative moMΦ. These were obtained after simultaneous nucleofection of both *mrc1* #1 and #2 gRNA, while MMR-positive moMΦ were obtained by nucleofection of an irrelevant control gRNA (Fig. 6D). These experiments demonstrated that the high colocalization between fucosylated nanocarriers and endosomal compartments observed in MMR-positive moMΦ was significantly reduced in MMR-negative moMΦ, as indicated by the decrease of PCC from 0.37 to 0.19 for Rab5 and from 0.36 to 0.24 for Rab7 (Fig. 6E). Thus, by using CRISPR/Cas9 gene knock-out we confirmed that the MMR delivers such fucosylated lipid nanocarriers into endosomal compartments of human moMΦ.

2.7. Levofloxacin encapsulated in fucosylated lipid nanocarriers inhibits mycobacterial growth more effectively than free antibiotics

To test the anti-mycobacterial potency of fucosylated lipid nanocarriers under in vitro conditions, they were loaded with levofloxacin, and the encapsulation efficiency was determined by HPLC-UV/Vis. MoMΦ or moDC were infected with GFP-labeled Bacillus Calmette-Guérin (BCG-GFP) at a multiplicity of infection (MOI) 1 or MOI 3, respectively, for 24 h and cells were then treated for 5 consecutive days with the indicated concentrations of levofloxacin, delivered either encapsulated in fucosylated lipid nanocarriers or as free antibiotics. At the end of the experiment, the percentage of GFP-positive cells was measured by flow cytometry. As similarly detected in both moMΦ and moDC (Fig. 7A), treatment with 10 μg/ml of encapsulated levofloxacin reduced the percentage of BCG-infected cells to 50%, whereas approx. 80% of the cells remained infected after treatment with the same amount of free levofloxacin. At the highest concentration of levofloxacin

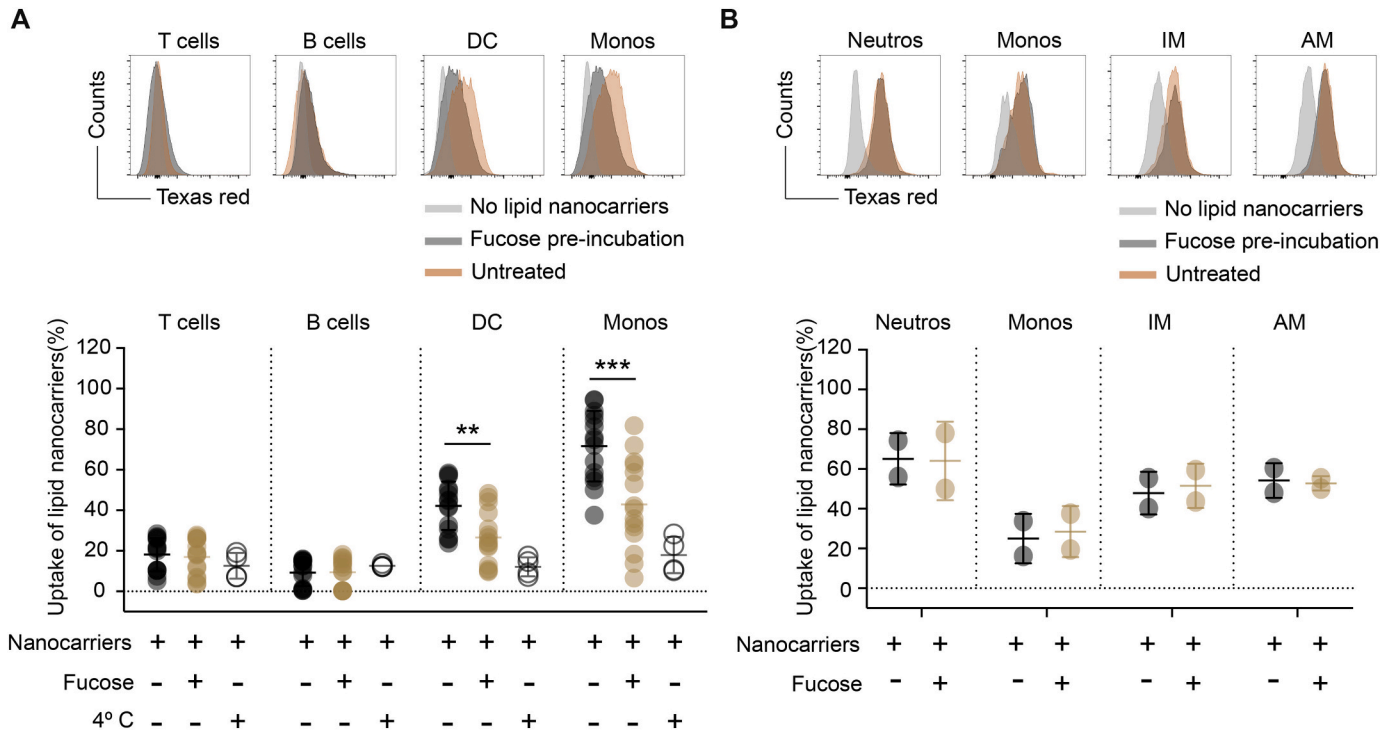

Fig. 4. Myeloid cells amongst PBMC or lung tissue show highest uptake of fucosylated lipid nanocarriers. Human PBMC or single-cell suspensions derived from human lung tissue were incubated with 250 μmol of carbohydrate-functionalized, Texas Red-labeled nanocarriers at 37 °C for 2 h. Where indicated, cells were incubated with 1 mM of L-fucose for 1 h prior to treatment with the lipid nanocarriers. As a negative control, incubation at 4 °C was performed. (A) Percentages of Texas Red-positive cells were determined for T cells, B cells, DC and monocytes within PBMC by flow cytometry. Histograms show representative data from one donor (upper panel). The lower panel depicts the quantification of Texas Red-positive cells. Error bars indicate means ± SEM (lower panel, two-tailed Wilcoxon test, $***P \leq 0.0015$, $**P \leq 0.0309$, $n = 4–15$, $N > 3$). (B) Percentages of Texas Red-positive monocytes, interstitial macrophages (IM) or alveolar macrophages (AM) derived from human lung tissue. Histograms show representative data from one donor (lower panel). (For interpretation of the references to colour in this figure legend, the reader is referred to the web version of this article.)

(i.e. 40 μg/ml), treatment with free levofloxacin did not further reduce the percentage of infected cells, while encapsulated antibiotics decreased the infection to approx. 8%. Thus, fucosylated lipid nanocarriers loaded with levofloxacin effectively inhibited the bacterial growth in BCG-infected myeloid cells with higher efficacy than the free antibiotics.

3. Discussion

Here we show that formulation of the second-line TB drug levofloxacin in fucosylated lipid nanocarriers increased its antimycobacterial activity while at the same time reducing its effective dose. These nanocarriers target MMR-positive myeloid cells such as AM and preferentially deliver their payload to endosomal compartments after MMR-mediated endocytosis. Hence, such fucosylated lipid nanocarriers provide a promising strategy to target AM, the natural niche for Mtb survival and propagation.

Given that TB drugs currently are administered systemically via the oral or intravenous routes and can cause severe off-target effects in non-infected organs (e.g., hepatotoxicity), there is a definitive need for new formulations of broadly used TB antibiotics [30,31]. Nanocarrier formulations using liposomal scaffolds are especially promising due to their size, hydrophobic/hydrophilic character and metabolizable components, which makes them highly biocompatible [32]. In addition, their surfaces can be functionalized for targeted cell-selective drug delivery [33,34]. In the present study, the second-line TB drug levofloxacin was formulated in fucosylated lipid nanocarriers. We thus aimed at targeting the MMR and other CLR expressed by AM, which are known to be the primary target and reservoir of Mtb [7,35–37].

Amongst PBMC and primary human lung cells treated with fucosylated nanocarriers, MMR-positive myeloid cells indeed demonstrated the highest nanocarrier uptake. Interestingly, this uptake was significantly reduced in monocytes and DC when PBMC were pre-incubated with soluble fucose, whereas this was not the case for lung-resident AM. As fucose binds with high affinity to CLR such as the MMR, addition of soluble fucose efficiently inhibits the interaction of CLR with carbohydrate structures [38]. Nevertheless, AM have a higher phagocytic capacity when compared with myeloid cells within PBMC, including unspecific CLR-independent uptake mechanisms [39]. Therefore, it seems likely that fucose alone does not efficiently block the overall uptake of fucosylated nanocarriers by AM. Additionally, during lung tissue digestion many cells die and release their content, which might in turn activate immune cells in the lung and augment their phagocytic capacity.

Our fucose inhibition studies suggested that primary human myeloid cells take up fucosylated lipid nanocarriers primarily by MMR-mediated endocytosis. The MMR is a phagocytic receptor with a cytoplasmic tail that contains a sequence of di-aromatic amino acids, which serves as an endosomal sorting signal and directs ligands to endosomal compartments [40]. Indeed, when addressing the subcellular localization of fucosylated nanocarriers in human moMΦ, we observed that these nanocarriers were preferentially found in endosomal compartments, which was inhibited by blocking the MMR (and other CLRs) with soluble fucose. Those observations were further confirmed by lack of preferential localization of fucosylated nanocarriers in endosomal compartments in primary human moMΦ in which MMR was ablated using CRISPR/Cas9-mediated gene editing.

Indeed, fucosylated lipid nanocarriers interact with several CLRs besides MMR, including DC-SIGN and MGL, as indicated by FACS analysis with CLR-hFc constructs. Functionalizing nanocarriers with

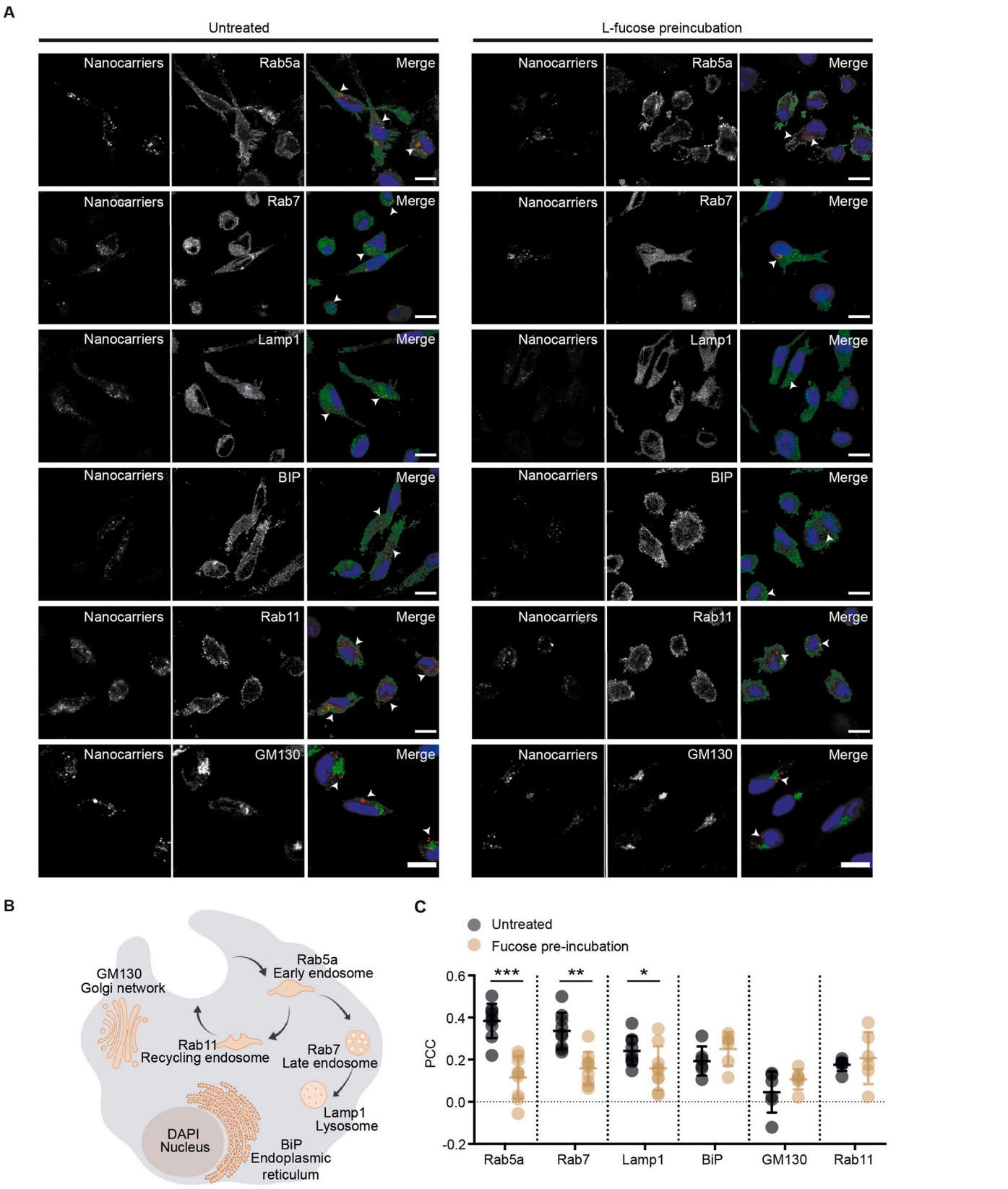

Fig. 5. Fucosylated lipid nanocarriers are preferentially delivered to endosomal compartments within human moMΦ. (A) Monocyte-derived macrophages (moMΦ) were incubated with 250 μmol of fucosylated, Texas Red-labeled lipid nanocarriers at 37 °C for 1 h. Where indicated, cells were incubated with 1 mM of L-fucose for 1 h prior to treatment. Organelle-specific markers in fixed moMΦ were stained for confocal microscopy. Scale bar: 10 μm. (B) Schematic depiction of the organelle-specific immunolabeling used for confocal analysis. Created with Biorender.com (C) Pearson's correlation coefficient (PCC) between Texas Red fluorescence derived from internalized targeted or non-targeted nanocarriers and labeled subcellular compartments was calculated for both conditions. For each donor, a minimum of three photomicrographs was analyzed, each of them comprising 5–10 cells. The error bars indicate mean ± SD (paired *t*-test, $^{***}P < 0.0001$, $^{**}P < 0.0017$, $^{*}P < 0.0419$, $n = 6$, $N = 2$). (For interpretation of the references to colour in this figure legend, the reader is referred to the web version of this article.)

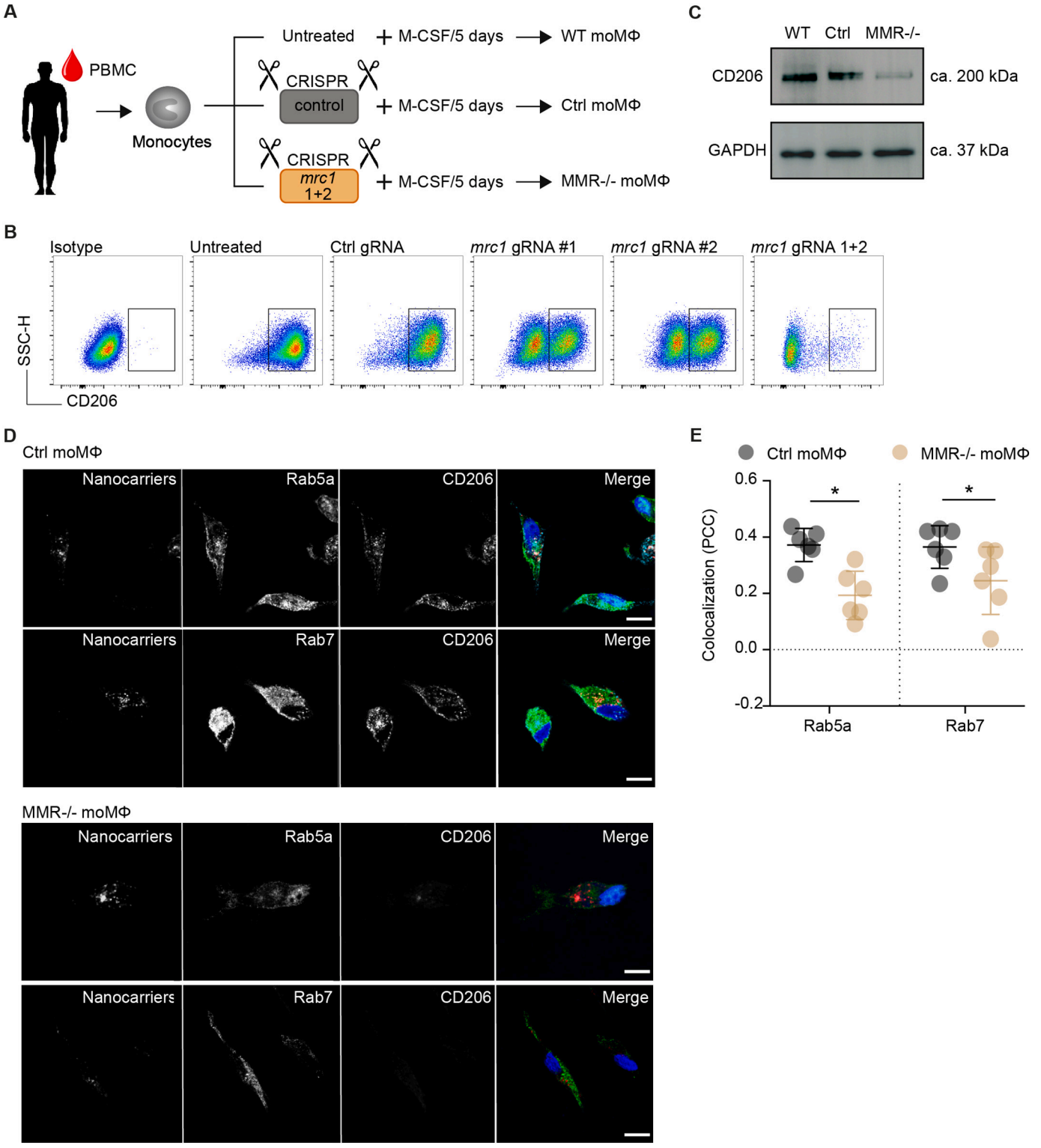

Fig. 6. Transport of fucosylated lipid nanocarriers to endosomal compartments of monocyte-derived macrophages depends on MMR expression. (A) Schematic depiction of the CRISPR/Cas9 gene editing strategy using Cas9 ribonucleoproteins (RNP) in human monocyte derived macrophages (moMΦ). (B) Western blot analysis of CD206 in MMR$^-$ moMΦ generated by simultaneous nucleofection with gRNA #1 and gRNA #2 RNPs. GAPDH was used as a loading control. (C) Dot plots from one representative donor show MMR cell surface expression before and after CRISPR/Cas9-mediated deletion using two different gRNA targeting the MMR as well as an irrelevant control gRNA. (D) MMR$^-$ moMΦ were incubated with fucosylated lipid nanocarriers for 2 h at 37 °C and Rab5 and Rab7 were immunolabeled as markers for early and late endosomes, respectively. Confocal microscopy analysis was performed and representative photomicrographs show fucosylated lipid nanocarriers in red and the immunolabeled markers in green. Scale bar: 10 μm. (E) PCC between Texas Red fluorescence derived from internalized nanocarriers and labeled subcellular compartments was calculated. For each donor a minimum of three photomicrographs was analyzed, each photo comprising 5–10 cells. Error bars indicate means ± SD (paired *t*-test, $^*P < 0.0225$, $^*P < 0.0326$, $n = 6$, $N = 2$). (For interpretation of the references to colour in this figure legend, the reader is referred to the web version of this article.)

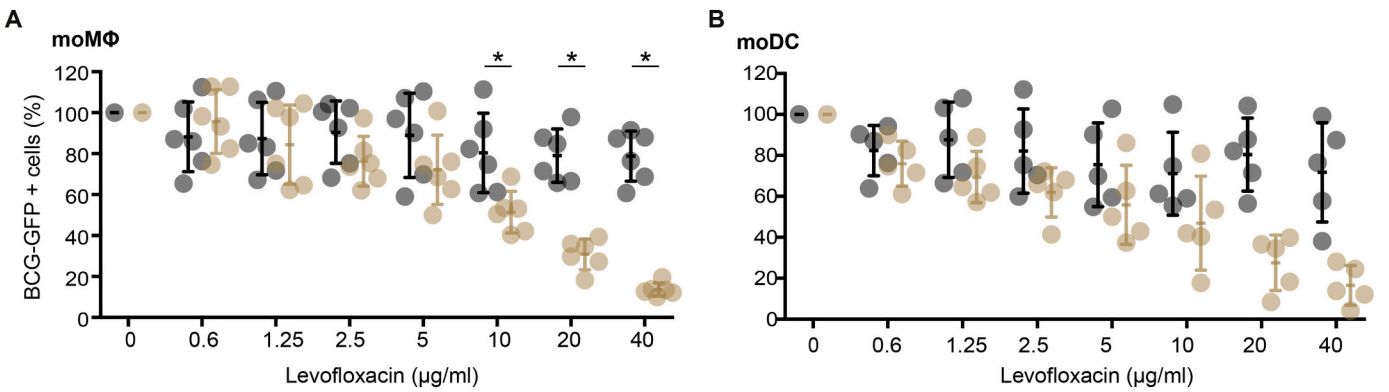

Fig. 7. Treatment with levofloxacin-loaded, fucosylated lipid nanocarriers effectively inhibits mycobacterial growth in both monocyte-derived myeloid cells. (A) Monocyte-derived macrophages (moMΦ) and (B) dendritic cells (moDC) were infected with BCG-GFP for 24 h at MOI 1 or 3, respectively. Cells were treated for 5 consecutive days with increasing concentrations of levofloxacin, delivered either encapsulated in fucosylated lipid nanocarriers (orange) or free form (grey). After treatment, percentages of GFP-positive cells were determined by flow cytometry and results were normalized by setting the percentage from the untreated sample as 100% (two-tailed Wilcoxon test, $*P \leq 0.0312$, $n = 5–6$, $N = 3$).

carbohydrates might further enhance the CLR targeting, as it was shown for other receptors that upon binding of natural ligands, receptor recycling is augmented and thus the number of surface receptor molecules is increased [41]. In contrast, functionalization with CLR-specific monoclonal antibodies was shown to reduce the recycling ability of these receptors and decrease the overall surface expression, hence resulting in reduced antigen internalization [42]. Additionally, compared with monoclonal antibodies, carbohydrate ligands have a lower risk of side effects as their production relies entirely on chemical methods, and their properties can be finely tuned to optimize the targeting, i.e. by modifying the saccharides' conformation and spatial orientation [43–45]. Conversely, targeting the MMR might also offer new strategies to modulate immune responses against TB, as previous studies have shown that interaction with MMR may suppress the release of selected proinflammatory cytokines and hence may regulate innate inflammatory responses [46,47].

Although previous studies addressed the targeting of AM by carbohydrate-functionalized nanocarriers [48–50], none of those investigations tested the capacity of such nanocarriers to deliver antibiotics and to clear mycobacterial infections. Here, fucosylated lipid nanocarriers were loaded with levofloxacin, as this fluoroquinolone is approved as a second-line antibiotic for treating MDR-TB [51,52]. Levofloxacin has to be employed at high daily doses of between 750 and 1000 mg [53], due to its poor cellular accumulation and sub-optimal pharmacokinetics and pharmacodynamics [54]. When applied to BCG-infected human moMΦ or moDC, the nano-formulation of levofloxacin decreased the percentage of BCG-infected cells more effectively than equal amounts of free antibiotics. As mycobacteria survive in phagosomes that do not fuse with late endosomal compartments while still retaining access to early endosomal compartments [55–57], it can be hypothesized that the preferred accumulation of the fucosylated nanocarriers in early endosomes enhances the antibiotics' efficacy against Mtb.

A possible therapeutic application of such fucosylated, antibiotic loaded nanocarriers would mimic the route of an Mtb infection. After inhalation, AM would be targeted and the carriers will eventually accumulate in endosomal compartments. Here, the payload is released and the residing bacteria are exposed to a high antibiotic concentration. It could be envisioned, therefore, that fucosylated lipid nanocarriers, called CLR-TargoSpheres [24], could serve for the selective delivery of antibiotics that usually are effective only at high dosage, provoke severe side effects and/or cannot cross cell membranes, hence reducing the absolute amount of antibiotics needed and improving their therapeutic window. This holds promise to significantly diminish the imminent complications of current TB treatment standards, increase patient compliance and restrain the emergence of resistant Mtb strains.

4. Material and methods

4.1. Ethics statement

Human lung lobes were acquired from patients who underwent lung resection for cancer or fibrosis. These experiments were approved by the ethics committee of the Medical School Hannover (Germany) and are in accordance with The Code of Ethics of the World Medical Association (number 2701–2015). All patients or their next of kin, caretakers, or guardians gave written informed consent for using lung tissue for research.

4.2. Human lung tissue

Lung tissue was obtained from patients undergoing surgical resection. Samples were transported in physiological saline solution (0.9% NaCl), which was kept for subsequent cell isolation. After removing necrotic sections, tissue (3–8 g) was mechanically disaggregated with the gentle MACS dissociator (Miltenyi Biotec, Bergisch Gladbach, Germany). Samples were then enzymatically digested with Dispase II, Collagenase/Dispase (Roche, Basel, Switzerland) and DNAse I (Sigma-Aldrich, Darmstadt, Germany) for 2 h at 37 °C, and medium RPMI 1640 with 10% FCS was added to stop the enzymatic reaction. Cell suspensions were combined with the lung transport medium and passed through 100 μm and 70 μm filters. After washing with PBS/BSA 1%, red blood cells were lysed using 5 ml of ammonium-chloride-potassium (ACK) lysing buffer for 5 min on ice. RPMI 1640 medium with 10% FCS was added to stop the enzymatic reaction and, after washing, cells were counted and used immediately.

4.3. Preparation and characterization of fucosylated lipid nanocarriers

The fucosylated nanocarriers employed in this work were CLR-TargoSpheres [24]. TargoSpheres® is the umbrella term for various lipid based nanocarriers developed by Rodos Biotarget. For preparing such fucosylated lipid nanocarriers, the basic nanocarrier scaffold and composition of liposomes was applied as well as methods to produce them. Accordingly, the particles were prepared with the thin-film hydration method followed by extrusion[58]. In brief, lipids and fucosylated residues (Rodos Biotarget GmbH) were dissolved in chloroform and ethanol, respectively. The stock solutions were then combined in a round-bottom flask, and the organic solvents were removed using a rotary evaporator. The flask was then transferred to a vacuum desiccator

and dried in vacuum for two days to remove any residual solvent. The final lipid film contained 8% (mole percent) of fucosyl targeting residue. The dry film was hydrated with a levofloxacin hydrochloride solution (approx. 110 g/l in PBS; 1 ml solution per 50 mg lipid film) for about 10 min and then sonicated at 35 °C until a homogeneous, milky solution was obtained. The crude sample was then extruded (30×) through a polycarbonate membrane (Whatman® Nuclepore™ Track-Etched Membrane) with a pore size of 200 nm followed by an extrusion through 50 nm (31×) using a hand-held LiposoFast extruder (AVESTIN Europe GmbH, Mannheim, Germany). Finally, the sample was dialyzed (RC membrane, MWCO 12000–14,000) against PBS (pH = 7.4) overnight to remove non-encapsulated levofloxacin. Lipid compositions and lipid concentrations were determined by high-performance thin-layer chromatography (HPTLC). To this end, the liposomal preparations were first lysed by methanol dilution to obtain concentrations of between 15 mg/l to 80 mg/l for the individual lipids, respectively. HPTLC Silica gel 60 plates (20 × 10 cm; Merck, Darmstadt, Germany) were pre-washed with methanol before spotting the samples and calibration standard with a Linomat IV semi-automatic sample applicator (CAMAG, Berlin, Germany). A five-point calibration ($n = 2$) was used. After drying, the plates were developed twice in an Automatic Developing Chamber 2 (ADC2; CAMAG) at 35% to 40% relative humidity and 25 ± 2 °C. The first run (85 mm) was used to separate cholesterol from the phospholipids (1 vol. *n*-hexane, 8 vol. acetone). The second run (50 mm) separated the individual lipids (25 vol. ethyl acetate, 25 vol. isopropanol, 13 vol. acetone, 8 vol. water, 8 vol. formic acid). For derivatization, the plate was briefly immersed in an acidic copper(II) sulfate solution (100 g/l $CuSO_4$ and 80 ml/l 85% H_3PO_4) and dried for 20 min. The dry plate was then placed on a Plate Heater III (CAMAG) preheated to 140 °C for 10 min. After cooling, the plate was read with a TLC Scanner 3 scanning densitometer (CAMAG) with the following settings: $\lambda = 365$ nm, absorption/reflection mode, slit dimensions 4.00 × 0.30 mm (micro), scanning speed 10 mm/s, data resolution 100 μm/step, detector mode automatic. The measurement data, i.e., the peak areas, were exported from winCATS (CAMAG) and imported in MS Excel. A second-degree polynomial was fitted to the calibration data and used for calculating the lipid concentrations of the formulations.

The size, size-distribution, PDI, and zeta potential of the final formulation were determined by dynamic light scattering (DLS) using a Zetasizer Nano ZS Series (Malvern Instruments Limited, Malvern, UK). To characterize their morphology, lipid nanocarriers were negatively stained with 2% uranyl acetate and analyzed by transmission electron microscopy (TEM; Tecnai™ G2 F20, Thermo Fisher Scientific, Waltham, USA). Finally, the nanocarrier particle concentration was determined by nanoparticle tracking analysis (NTA) using a NanoSight LM 10 (Malvern Instruments Limited).

Fucosylation of nanocarriers was verified by using a flow cytometry-based method. Fucosylated lipid nanocarriers were incubated for 30 min at 4 °C with increasing concentrations of a FITC-coupled *Aleuria aurantia* lectin (AAL). After washing of unbound lectin, FITC signal was determined by flow cytometry as a measure of the density of the fucosyl residues on the surface of the nanocarriers.

Next, the CLR binding profile of fucosylated lipid nanocarriers was determined using CLR-hFc fusion proteins [53–55]. Briefly, 10 mM of fucosylated lipid nanocarriers were initially washed with lectin binding buffer (50 mM HEPES, 5 mM $MgCl_2$, 5 mM $CaCl_2$, pH 7.4) and placed in a round-bottom 96-well plate. After incubation with 300 ng of CLR-hFc fusion protein in 100 μl of lectin binding buffer for 1 h at 4 °C, the lipid nanocarriers were then washed one time with lectin binding buffer and then suspended in 50 μl of Alexa Fluor 647-conjugated (1:100 dilution) goat anti-human Fc antibody (Dianova, Hamburg, Germany). After 30 min incubation at 4 °C, lipid nanocarriers were washed once with lectin binding buffer and flow cytometry measurements were performed using Attune NxT Flow Cytometer (ThermoFisher Scientific, Darmstadt, Germany). Binding of fucosylated lipid nanocarriers to MMR-hFc fusion proteins could not be tested, because generation of MMR-hFc was not possible. This was due to the fact that the MMR is composed of 8 consecutive carbohydrate-recognition domains (CRD), which would require expression of a single CRD together with the hFc moiety. However, such an approach would disregard the valency strength of MMR.

4.4. Isolation of primary human immune cells from blood

Human PBMC were isolated from buffy coats of healthy blood donors provided by the blood bank Springe (Springe, Germany) via Ficoll density gradient centrifugation (Biochrom AG, Berlin, Germany). CD14-positive monocytes were isolated by positive MACS selection using CD14 MicroBeads (Miltenyi Biotec). To differentiate monocyte-derived dendritic cells (moDC) and macrophages (moMΦ), purified monocytes were cultivated for 5 days in serum-free DC CellGro® medium (CellGenix, Freiburg, Germany) enriched with 1000 U/ml granulocyte-macrophage colony stimulating factor (GM-CSF; CellGenix) and 1000 U/ml interleukin 4 (IL-4; CellGenix) for moDC, and 100 ng/ml macrophage colony stimulating factor (M-CSF; Miltenyi Biotec), respectively.

4.5. Isolation of primary human immune cells from secondary lymphoid organs

Human tonsils and lymph nodes were obtained from patients undergoing surgical resection. After removing necrotic sections, tissue (1–5 g) was mechanically disaggregated with the gentle MACS dissociator. Samples were then enzymatically digested with 2.6 WU/ml of Liberase TL (Sigma-Aldrich) for 30 min at 37 °C, and 10 mM EDTA was added to stop the enzymatic reaction. Cell suspensions were filtered through 100 μm and 70 μm strainers, and after washing, cells were counted and used immediately.

4.6. Flow cytometry

5×10^5 cells derived from human lung tissue were stained with the Zombie Aqua™ live/dead fixable dye (Biolegend, San Diego, USA) and immunolabeled with anti-CD45-PeCy5.5 (HI30, Thermofisher Scientific), anti-HLA-DR-APC-Cy7 (L243; Biolegend), anti-CD15-PacBlue, anti-CD169-PE (7–239; Biolegend), and anti-CD11b-BV605 (M1/70; Biolegend) for 15 min at 4 °C. For nanocarrier uptake studies, 1×10^6 PBMC were immunolabeled with anti-CD3-PerCP (UCHT1, Biolegend), anti-CD14-PacBlue (M5E2, Biolegend), anti-CD19-Amcyan (HIB19, BD Biosciences), and anti-HLA-DR-APC-Cy7 (L243; Biolegend). For C-type lectin characterization studies, 5×10^5 cells were stained with anti-CD206-PE-Cy7 (15–2; Biolegend), anti-CD205-FITC (MG38; eBioscience, San Diego, USA) and anti-CD209-APC (9E9A8; Biolegend). Unspecific immunolabeling conferred by Fc receptor binding was blocked by the addition of 10% Gamunex solution (Grifols Deutschland GmbH, Frankfurt am Main, Germany). Data were acquired on a LSR-II flow cytometer (BD Biosciences, New Jersey, USA) and analyzed with the FlowJo software (Tree Star).

4.7. Levofloxacin encapsulation efficiency

A 10 mM solution of fucosylated lipid nanocarriers loaded with levofloxacin was diluted in ethanol in order to release the levofloxacin. An additional aliquot of the formulation was ultra-filtrated using Centrisart® I 300,000 MWCO tubes (Sartorius, Göttingen, Germany) for 30 min at 300 x g in order to separate the nanocarriers from the dispersant. The permeate was collected and used to determine the amount of free levofloxacin in the formulation. Quantification was performed by HPLC-UV/Vis on a system equipped with a Dionex P680 pump and a Dionex 170 U UV detector (Thermo Fisher Scientific) using a 30 × 2.1 mm Kinetex® core-shell column (2.6 μm; Phenomenex, Torrance, USA). The mobile phase used for this separation was MeOH +0.1% formic acid (FA): Water +0.1% FA (50:50 *v*/v). The flow rate throughout the analysis was 300 μl/min, and UV detection was performed at 294 nm.

4.8. Confocal fluorescence microscopy

For confocal imaging, moMΦ were seeded in μ-Slide 8-well culture chambers (Ibidi GmbH, Gräfelfing, Germany) during the five days of differentiation. After nanocarrier treatment, cells were fixed with 3% paraformaldehyde for 10 min at room temperature, washed three times with PBS and blocked with glycine-containing blocking buffer for 1 h. Cells were washed again three times with PBS and incubated with primary antibodies of interest for 24 h at 4 °C. After PBS washing, fluorophore-conjugated secondary antibodies were added and the samples were incubated for 2 h at room temperature. DAPI was added for nuclear staining, and the cells were washed and mounted with DAKO fluorescent mounting medium. Confocal microscopy was then performed with the Olympus FV1000-IX81 laser-scanning microscope using the 60× oil immersion objective, NA 1.35.

4.9. Fucose blocking

Prior to treatment of cells with lipid nanocarriers, medium was exchanged and replaced with fresh CellGro medium containing 1 mM of L-Fucose (Sigma-Aldrich). After 1 h of incubation, 250 μmol of lipid nanocarriers were added to the fucose-containing medium and after the indicated time points, cells were washed twice with cold PBS to remove membrane-bound nanocarriers.

4.10. CRISPR/Cas9 gene editing

For CRISPR/Cas9 gene knockout of CD206, ribonucleoprotein (RNP) complexes consisting of Cas9 nuclease (Integrated DNA Technologies Inc.; IDT) and targeting guide RNA (gRNA; annealed crRNA and tracrRNA; both IDT) were used. Human *mrc1* crRNAs were selected from pre-designed crRNAs from the Broad Institute of Harvard and MIT (Genscript; www.genscript.com/gRNA-database.html). To assemble crRNA:tracrRNA complexes, two anti-hMMR crRNA (#1: 5'-CCCAGTAGGAGAACAGCACC-3′ and #2: 5'-CCAGCCATGTATACGCTACT-3′) were individually mixed with unmodified tracrRNA in 1:1 M (210 pmol) ratio, heated at 95 °C for 5 min and slowly cooled down to room temperature. Formed crRNA:tracrRNA complexes were then used individually or pooled together for RNP assembly. To form the RNP, Cas9 NLS protein from *S. pyogenes* was added in 3:1 M ratio and the mixture was left at room temperature for 10–20 min. As a control, a negative control crRNA (IDT) without specificity for the mouse, rat or human genomes was used to prepare Cas9 RNPs as described above.

Directly after monocyte isolation, cells were transfected with RNP of interest using the Primary Cell 3D-Nucleofector X kit L (Lonza) using a 4D nucleofector X and Core units (both Lonza). Briefly, for each nucleofection 3 ml of complete medium was pre-warmed in the cell incubator. Up to 1×10^6 freshly isolated monocytes were resuspended in 100 μl of primary cell nucleofection solution, added to the cuvette pre-loaded with total of 10 μl of RNP and immediately electroporated using pulse program EA100. Afterwards, pre-warmed complete medium was used to seed nucleofected monocytes for differentiation as described above.

4.11. Western blot analysis

Cells were lysed in reducing SDS sample buffer, treated for 20 min with benzonase (Merck, Darmstadt, Germany) at RT and then denatured at 65 °C for 10 min. Lysates were applied on 10% Tris-glycine gels and blotted on PVDF membrane. Membrane was blocked in 5% milk in TBS-T and incubated with rabbit anti-human CD206 (Abcam) for 2 h. Subsequently, membrane was incubated for 1 h at RT with goat anti-rabbit HRP (Merck) and developed with Clarity Western ECL Reagent (BioRad, Hercules, USA). For GAPDH, membrane was incubated for 2 h at RT with anti-GAPDH-HRP (Biolegend) in 3% BSA in TBS-T.

Data availability statement

The authors confirm that the data supporting the findings of this study are available within the article and its supplementary materials.

Declaration of Competing Interest

CH and MF are employees of Rodos Biotarget GmbH, which holds intellectual property on targeted nanocarrier technology. All other authors declare no conflict of interest.

Acknowledgements

We thank L. de Araujo, K. Baumann and P. Blank for help with the experiments and for scientific discussions. This work was supported by the German Federal Ministry of Economics and Technology (BMWi), via the Consortium of Industrial Research Associations (AiF), ZIM Program, Grant KF2531702AJ3 ["Development of biocompatible, antibiotic-loaded nanocarriers (TargoSpheres®) specific for pulmonary antigen-presenting cells for intracellular release of the antibiotic"] to MF, and Grant KF3134203AJ3 ["Preclinical analysis of the applicability and efficacy of antibiotic-loaded TargoSpheres® (TS/AB) for treating mycobacterial infections in novel mouse models"] to MF and UK; by the Ministry for Science and Culture of Lower Saxony (research consortium COALITION) to RF and UK; by the Deutsche Forschungsgemeinschaft (DFG, German Research Foundation) grant SFB807-P16 to RT, grant SFB900-B1 to RF, grant SFB900-B2 to UK; by the Deutsche Forschungsgemeinschaft under Germany's Excellence Strategy – EXC 2155 "RESIST" – Project ID 39087428 to RF and UK.

Appendix A. Supplementary data

Supplementary data to this article can be found online at https://doi.org/10.1016/j.jconrel.2021.04.012.

References

[1] WHO, Global tuberculosis report 2019, World Health Organization, 2019. Retrieved from, https://apps.who.int/iris/bitstream/handle/10665/329368/9789241565714-eng.pdf?ua=1.
[2] WHO, Guidelines for treatment of drug-susceptible tuberculosis and patient care, World Health Organization, 2017. Retrieved from: https://apps.who.int/iris/bitstream/handle/10665/255052/9789241550000-eng.pdf?sequence=1.
[3] WHO, Multidrug-resistant Tuberculosis (MDR-TB), World Health Oranization, 2018. Retrieved from: https://www.who.int/tb/areas-of-work/drug-resistant-tb/MDR-RR_TB_factsheet_2018_Apr2019.pdf.
[4] R. Sharma, A. Kaur, A.K. Sharma, N. Dilbaghi, A.K. Sharma, Nano-based anti-tubercular drug delivery and therapeutic interventions in tuberculosis, Curr. Drug Targets 18 (2017) 72–86, https://doi.org/10.2174/1389450116666150804110238.
[5] A. Costa, M. Pinheiro, J.A. Magalhães, R. Ribeiro, V. Seabra, S. Reis, B. Sarmento, The formulation of nanomedicines for treating tuberculosis, Adv. Drug Deliv. Rev. 102 (2016) 102–115, https://doi.org/10.1016/j.addr.2016.04.012.
[6] I.P. Kaur, H. Singh, Nanostructured drug delivery for better management of tuberculosis, J. Control. Release 184 (2014) 36–50, https://doi.org/10.1016/j.jconrel.2014.04.009.
[7] S.B. Cohen, B.H. Gern, J.L. Delahaye, K.N. Adams, C.R. Plumlee, J.K. Winkler, D. R. Sherman, M.Y. Gerner, K.B. Urdahl, Alveolar macrophages provide an early *Mycobacterium tuberculosis* niche and initiate dissemination, Cell Host Microbe 24 (2018), https://doi.org/10.1016/j.chom.2018.08.001, 439–446.e434.
[8] S.H. Kaufmann, How can immunology contribute to the control of tuberculosis? Nat Rev Immunol 1 (2001) 20–30, https://doi.org/10.1038/35095558.
[9] C.J. Cambier, S. Falkow, L. Ramakrishnan, Host evasion and exploitation schemes of *Mycobacterium tuberculosis*, Cell 159 (2014) 1497–1509, https://doi.org/10.1016/j.cell.2014.11.024.
[10] J. Pieters, *Mycobacterium tuberculosis* and the macrophage: maintaining a balance, Cell Host Microbe 3 (2008) 399–407, https://doi.org/10.1016/j.chom.2008.05.006.
[11] S. Goyal, T.E. Klassert, H. Slevogt, C-type lectin receptors in tuberculosis: what we know, Med microbiol and immunol 205 (2016) 513–535, https://doi.org/10.1007/s00430-016-0470-1.
[12] M.J. Marakalala, H. Ndlovu, Signaling C-type lectin receptors in antimycobacterial immunity, PLoS Pathog. 13 (2017), e1006333, https://doi.org/10.1371/journal.ppat.1006333.

[13] H. Yan, T. Kamiya, P. Suabjakyong, N.M. Tsuji, Targeting C-type lectin receptors for cancer immunity, Front Immunol 6 (2015), https://doi.org/10.3389/fimmu.2015.00408.

[14] T. Frenz, E. Grabski, V. Durán, C. Hozsa, A. Stepczynska, M. Furch, R.K. Gieseler, U. Kalinke, Antigen presenting cell-selective drug delivery by glycan-decorated nanocarriers, Eur. J. Pharm. Biopharm. 95 (2015) 13–17, https://doi.org/10.1016/j.ejpb.2015.02.008.

[15] D. van Dinther, D.A. Stolk, R. van de Ven, Y. van Kooyk, T.D. de Gruijl, J.M.M. den Haan, Targeting C-type lectin receptors: a high-carbohydrate diet for dendritic cells to improve cancer vaccines, J. Leukoc. Biol. 102 (2017) 1017–1034, https://doi.org/10.1189/jlb.5MR0217-059RR.

[16] T. Johannssen, B. Lepenies, Glycan-based cell targeting to modulate immune responses, Trends Biotechnol. 35 (2017) 334–346, https://doi.org/10.1016/j.tibtech.2016.10.002.

[17] J. Shao, J.K.H. Ma, Characterization of a mannosylphospholipid liposome system for drug targeting to alveolar macrophages, Drug Deliv 4 (1997) 43–48, https://doi.org/10.3109/10717549709033187.

[18] M. Rajaram, B. Ni, T. Carlson, L.S. Schlesinger, Mannose receptor (CD206)-mediated signaling in human macrophages in the context of tuberculosis, J Immunol 192 (2014), 186.19.

[19] B.K. Kang, L.S. Schlesinger, Characterization of mannose receptor-dependent phagocytosis mediated by *Mycobacterium tuberculosis* lipoarabinomannan, Infect. Immun. 66 (1998) 2769–2777.

[20] P.B. Kang, A.K. Azad, J.B. Torrelles, T.M. Kaufman, A. Beharka, E. Tibesar, L. E. DesJardin, L.S. Schlesinger, The human macrophage mannose receptor directs *Mycobacterium tuberculosis* lipoarabinomannan-mediated phagosome biogenesis, J. Exp. Med. 202 (2005) 987–999, https://doi.org/10.1084/jem.20051239.

[21] A.K. Azad, M.V. Rajaram, L.S. Schlesinger, Exploitation of the macrophage mannose receptor (CD206) in infectious disease diagnostics and therapeutics, J Cytol Mol Biol 1 (2014) 1000003, https://doi.org/10.13188/2325-4653.1000003.

[22] W. Wijagkanalan, S. Kawakami, M. Takenaga, R. Igarashi, F. Yamashita, M. Hashida, Efficient targeting to alveolar macrophages by intratracheal administration of mannosylated liposomes in rats, J. Control. Release 125 (2008) 121–130, https://doi.org/10.1016/j.jconrel.2007.10.011.

[23] A.V. Chavez-Santoscoy, R. Roychoudhury, N.L. Pohl, M.J. Wannemuehler, B. Narasimhan, A.E. Ramer-Tait, Tailoring the immune response by targeting C-type lectin receptors on alveolar macrophages using “pathogen-like” amphiphilic polyanhydride nanoparticles, Biomaterials 33 (2012) 4762–4772, https://doi.org/10.1016/j.biomaterials.2012.03.027.

[24] Rodos Biotarget, TargoSpheres®: Nanocarriers for targeted drug delivery, 2021. Retrieved from, http://www.biotargeting.eu.

[25] R.W. Stokes, R. Norris-Jones, D.E. Brooks, T.J. Beveridge, D. Doxsee, L.M. Thorson, The glycan-rich outer layer of the cell wall of *Mycobacterium tuberculosis* acts as an antiphagocytic capsule limiting the association of the bacterium with macrophages, Infect. Immun. 72 (2004) 5676–5686, https://doi.org/10.1128/iai.72.10.5676-5686.2004.

[26] J.T. Monteiro, K. Schön, T. Ebbecke, R. Goethe, J. Ruland, W. Baumgärtner, S. C. Becker, B. Lepenies, The CARD9-associated C-type lectin, Mincle, recognizes La Crosse virus (LACV) but plays a limited role in early antiviral responses against LACV, Viruses 11 (2019) 303, https://doi.org/10.3390/v11030303.

[27] S. Mayer, R. Moeller, J.T. Monteiro, K. Ellrott, C. Josenhans, B. Lepenies, C-type lectin receptor (CLR)-Fc fusion proteins as tools to screen for novel CLR/bacteria interactions: an exemplary study on preselected *Campylobacter jejuni* isolates, Front. Immunol. 9 (2018) 213, https://doi.org/10.3389/fimmu.2018.00213.

[28] M. Maglinao, M. Eriksson, M.K. Schlegel, S. Zimmermann, T. Johannssen, S. Götze, P.H. Seeberger, B. Lepenies, A platform to screen for C-type lectin receptor-binding carbohydrates and their potential for cell-specific targeting and immune modulation, J. Control. Release 175 (2014) 36–42, https://doi.org/10.1016/j.jconrel.2013.12.011.

[29] K.W. Dunn, M.M. Kamocka, J.H. McDonald, A practical guide to evaluating colocalization in biological microscopy, Am J Physiol Cell Physiol 300 (2011) C723–C742, https://doi.org/10.1152/ajpcell.00462.2010.

[30] P. Blasi, A. Schoubben, S. Giovagnoli, C. Rossi, M. Ricci, Fighting tuberculosis: old drugs, new formulations, Expert Opin Drug Deliv 6 (2009) 977–993, https://doi.org/10.1517/17425240903130577.

[31] D. Traini, P.M. Young, Drug delivery for tuberculosis: is inhaled therapy the key to success? Ther. Deliv. 8 (2017) 819–821, https://doi.org/10.4155/tde-2017-0050.

[32] Volkmar Weissig (Ed.), Liposomes: Methods and Protocols vol 1, Humana Press, New Jersey, 2010, https://doi.org/10.1007/978-1-60327-360-2.

[33] L. Shang, K. Nienhaus, G.U. Nienhaus, Engineered nanoparticles interacting with cells: size matters, J Nanobiotechnology 12 (2014) 5, https://doi.org/10.1186/1477-3155-12-5.

[34] L. Sercombe, T. Veerati, F. Moheimani, S.Y. Wu, A.K. Sood, S. Hua, Advances and challenges of liposome assisted drug delivery, Front. Pharmacol. 6 (2015) 286, https://doi.org/10.3389/fphar.2015.00286.

[35] G. Lugo-Villarino, D. Hudrisier, A. Tanne, O. Neyrolles, C-type lectins with a sweet spot for *Mycobacterium tuberculosis*, Eur J Microbiol Immunol (Bp) 1 (2011) 25–40, https://doi.org/10.1556/EuJMI.1.2011.1.6.

[36] L.S. Schlesinger, S.R. Hull, T.M. Kaufman, Binding of the terminal mannosyl units of lipoarabinomannan from a virulent strain of *Mycobacterium tuberculosis* to human macrophages, J. Immunol. 152 (1994) 4070–4079.

[37] M. Woo, C. Wood, D. Kwon, K.H.P. Park, G. Fejer, V. Delorme, *Mycobacterium tuberculosis* infection and innate responses in a new model of lung alveolar macrophages, Front Immunol 9 (2018), https://doi.org/10.3389/fimmu.2018.00438.

[38] R.T. Lee, T.L. Hsu, S.K. Huang, S.L. Hsieh, C.H. Wong, Y.C. Lee, Survey of immune-related, mannose/fucose-binding C-type lectin receptors reveals widely divergent sugar-binding specificities, Glycobiology 21 (2011) 512–520, https://doi.org/10.1093/glycob/cwq193.

[39] A. Schweizer, P.D. Stahl, J. Rohrer, A di-aromatic motif in the cytosolic tail of the mannose receptor mediates endosomal sorting, J. Biol. Chem. 275 (2000) 29694–29700, https://doi.org/10.1074/jbc.M000571200.

[40] L.J. Cruz, P.J. Tacken, J.M. Pots, R. Torensma, S.I. Buschow, C.G. Figdor, Comparison of antibodies and carbohydrates to target vaccines to human dendritic cells via DC-SIGN, Biomaterials 33 (2012) 4229–4239, https://doi.org/10.1016/j.biomaterials.2012.02.036.

[41] P.J. Tacken, M. Ter Huurne, R. Torensma, C.G. Figdor, Antibodies and carbohydrate ligands binding to DC-SIGN differentially modulate receptor trafficking, Eur. J. Immunol. 42 (1989-1998) 2012, https://doi.org/10.1002/eji.201142258.

[42] B. Lepenies, J. Lee, S. Sonkaria, Targeting C-type lectin receptors with multivalent carbohydrate ligands, Adv. Drug Deliv. Rev. 65 (2013) 1271–1281, https://doi.org/10.1016/j.addr.2013.05.007.

[43] Y. van Kooyk, W.W.J. Unger, C.M. Fehres, H. Kalay, J.J. García-Vallejo, Glycan-based DC-SIGN targeting vaccines to enhance antigen cross-presentation, Mol. Immunol. 55 (2013) 143–145, https://doi.org/10.1016/j.molimm.2012.10.031.

[44] M. Sanchez-Navarro, J. Rojo, Targeting DC-SIGN with carbohydrate multivalent systems, Drug News Perspect 23 (2010) 557–572, https://doi.org/10.1358/dnp.2010.23.9.1437246.

[45] J. Zhang, S.D. Tachado, N. Patel, J. Zhu, A. Imrich, P. Manfruelli, M. Cushion, T. B. Kinane, H. Koziel, Negative regulatory role of mannose receptors on human alveolar macrophage proinflammatory cytokine release in vitro, J. Leukoc. Biol. 78 (2005) 665–674, https://doi.org/10.1189/jlb.1204699.

[46] M. Chieppa, G. Bianchi, A. Doni, A. del Prete, M. Sironi, G. Laskarin, P. Monti, L. Piemonti, A. Biondi, A. Mantovani, M. Introna, P. Allavena, Cross-linking of the mannose receptor on monocyte-derived dendritic cells activates an anti-inflammatory immunosuppressive program, J. Immunol. 171 (2003) 4552–4560, https://doi.org/10.4049/jimmunol.171.9.4552.

[47] S. Kawakami, J. Wong, A. Sato, Y. Hattori, F. Yamashita, M. Hashida, Biodistribution characteristics of mannosylated, fucosylated, and galactosylated liposomes in mice, Biochim. Biophys. Acta 1524 (2000) 258–265, https://doi.org/10.1016/s0304-4165(00)00163-x.

[48] S.P. Vyas, Y.K. Katare, V. Mishra, V. Sihorkar, Ligand directed macrophage targeting of amphotericin B loaded liposomes, Int. J. Pharm. 210 (2000) 1–14.

[49] S. Chono, S. Tanino, T. Seki, K. Morimoto, Efficient drug targeting to rat alveolar macrophages by pulmonary administration of ciprofloxacin incorporated into mannosylated liposomes for treatment of respiratory intracellular parasitic infections, J. Control. Release 127 (2008) 50–58, https://doi.org/10.1016/j.jconrel.2007.12.011.

[50] J.A. Caminero, G. Sotgiu, A. Zumla, G.B. Migliori, Best drug treatment for multidrug-resistant and extensively drug-resistant tuberculosis, Lancet Infect. Dis. 10 (2010) 621–629, https://doi.org/10.1016/s1473-3099(10)70139-0.

[51] WHO, Guidelines for the programmatic management of drug-resistant tuberculosis, World Health Organization, 2011.

[52] A.D. Pranger, T.S. van der Werf, J.G.W. Kosterink, J.W.C. Alffenaar, The role of fluoroquinolones in the treatment of tuberculosis in 2019, Drugs 79 (2019) 161–171, https://doi.org/10.1007/s40265-018-1043-y.

[53] A.D. Pranger, J.W. Alffenaar, R.E. Aarnoutse, Fluoroquinolones, the cornerstone of treatment of drug-resistant tuberculosis: a pharmacokinetic and pharmacodynamic approach, Curr. Pharm. Des. 17 (2011) 2900–2930, https://doi.org/10.2174/138161211797470200.

[54] I. Vergne, R.A. Fratti, P.J. Hill, J. Chua, J. Belisle, V. Deretic, *Mycobacterium tuberculosis* phagosome maturation arrest: mycobacterial phosphatidylinositol analog phosphatidylinositol mannoside stimulates early endosomal fusion, Mol. Biol. Cell 15 (2004) 751–760, https://doi.org/10.1091/mbc.e03-05-0307.

[55] I. Vergne, M. Gilleron, J. Nigou, Manipulation of the endocytic pathway and phagocyte functions by *Mycobacterium tuberculosis* lipoarabinomannan, Front. Cell. Infect. Microbiol. 4 (2015) 187, https://doi.org/10.3389/fcimb.2014.00187.

[56] C. Bussi, M.G. Gutierrez, *Mycobacterium tuberculosis* infection of host cells in space and time, FEMS Microbiol. Rev. 43 (2019) 341–361, https://doi.org/10.1093/femsre/fuz006.

[57] H. Zhang, Thin-Film hydration followed by extrusion method for liposome preparation, Methods Mol Biol (Clifton, N.J.) 1522 (2017) 17–22, https://doi.org/10.1007/978-1-4939-6591-5_2.